Supporting Information

Efficient delivery of carotenoids to adipocytes with albumin

*Joanna Mazurkiewicz[a,b], Ewa Stanek[a,c], Aleksandra Kolodziejczyk[a,b], Marta Karpiel[a,b], Krzysztof Czamara[c], Tiago H. Ferreira[d], Pedro Maximiano[d], Pedro N. Simões[d], Igor Reva[d], Justyna Kalinowska-Tłuścik[b], and Agnieszka Kaczor[b,]**

[a] Jagiellonian University, Doctoral School of Exact and Natural Sciences, 11 Lojasiewicza Str., 30-348 Krakow, Poland.

[b] Jagiellonian University, Faculty of Chemistry, 2 Gronostajowa Str., 30-387 Krakow, Poland.

[c] Jagiellonian University, Jagiellonian Centre for Experimental Therapeutics (JCET), 14 Bobrzynskiego Str., 30-348 Krakow, Poland.

[d] University of Coimbra, CERES, Department of Chemical Engineering, 3030-790 Coimbra, Portugal.

Contents:

Figures		
	Description	**Page number**
Fig. S1	The Cambridge Structural Database search results for astaxanthin and its derivatives' crystal structures.	S4-S5
Fig. S2	Electronic absorption and ECD spectra of (3S,3'S)-AXT in PBS in the 300-700 nm range after the centrifugation.	S6
Fig. S3	Electronic absorption and ECD spectra of (3*S*,3'*S*)-AXT:BSA complexes and BSA in the range of 200-300 nm.	S6
Fig. S4	ECD spectra of (3*S*,3'*S*)-AXT:BSA complexes with a molar ratio of (3*S*,3'*S*)-AXT to BSA equal to 3:1 of several independently prepared samples.	S7
Fig. S5	Stability of the (3*S*,3'*S*)-AXT:BSA supramolecular complex monitored by electronic absorption and ECD spectra.	S8
Fig. S6	Comparison of reversed RROA and RR spectra for (3*S*,3'*S*)-AXT:BSA complexes.	S9
Fig. S7	Comparison of reversed RROA spectra for (3*S*,3'*S*)-AXT:BSA complexes with 1:1 and 3:1 CAR to BSA molar ratio.	S9
Fig. S8	Root mean square displacement (RMSD) of Cα of the BSA residues as a function of physical time and respective root mean square fluctuation (RMSF) for the 1:1 system.	S10
Fig. S9	RMSD of BSA backbone and (3*S*,3'*S*)-AXT molecules.	S10
Fig. S10	Secondary structure of BSA residues as a function of physical time and respective RMSF values for the 1:1 (a) and 3:1 (b) systems.	S11
Fig. S11	Evolution of the hydrogen bonds during the simulation time.	S12
Fig. S12	Number of salt bridges in BSA as a function of physical time.	S12
Fig. S13	Radius of gyration of BSA as a function of physical time.	S13
Fig. S14	Root mean square fluctuations of Cα of the BSA residues.	S13
Fig. S15	Mapping of RMSF values on the BSA structure.	S14
Fig. S16	Distances between the centre of mass (COM) of the bonded (3*S*,3'*S*)-AXT molecule and the COM of the binding pocket residues.	S14
Fig. S17	Minimum distances between AXT1 (AXT in the binding pocket) and selected residues of the BSA binding pocket at the start (t = 0 μs, blue dots) and at the end (t = 2 μs, red dots) of the simulation time for: (a) (3S,3'S) AXT:BSA = 1:1 ratio; and (b) (3S,3'S)-AXT:BSA = 3:1 ratio.	S15
Fig. S18	RMSD of Cα of the BSA regarding the binding pocket residues.	S16
Fig. S19	Secondary structure of the BSA regarding the binding pocket residues.	S16

Fig. S20	Number of BSA residues in contact with the two (3*S*,3'*S*)-AXT molecules in solution and secondary structure of BSA regarding the residues in contact with (3*S*,3'*S*)-AXT aggregate.	S17
Fig. S21	Hydrogen bonds between the (3*S*,3'*S*)-AXT aggregate and BSA residues.	S17
Fig. S22	Classification and illustration of the (3*S*,3'*S*)-AXT aggregates observed in the last μs of the trajectory.	S18
Fig. S23	RMSD of Cα of the BSA residues in contact with the (3*S*,3'*S*)-AXT aggregate observed for the 3:1 system.	S19
Fig. S24	Initial and final frames from the trajectory of an MD simulation for the 3:1 (3*S*,3'*S*)-AXT:BSA system without restraining the dihedrals in the polyene chain of (3*S*,3'*S*)-AXT.	S19
Fig. S25	Images of lipid distribution in primary adipocytes of white adipose tissue (eWAT) and brown adipose tissue (iBAT), after stimulation with (3*S*,3'*S*)-AXT dispersed in DMSO:water, for mice of different age, sex and using different laser power.	S20
Fig. S26	Time-dependent increase of (3*S*,3'*S*)-AXT level in primary adipocytes.	S20
Fig. S27	Changes in the position of marker band near 1516 cm^{-1} due to different forms of (3*S*,3'*S*)-AXT delivery.	S21
Tables		
	Description	**Page number**
Tab. S1	Ratios of the experimental integral intensity of the bands at 1516 cm^{-1} and 1160 cm^{-1} (I_{1516}/I_{1160}) for RR and RROA spectra for CAR to BSA molar ratios of 1:1 and 3:1.	S22
Tab. S2	Experimental ratios of CID values for bands at 1516 and 1160 cm^{-1}.	S22
Tab. S3	Comparison of (3*S*,3'*S*)-AXT content in adipocytes depending on the presence of BSA as a carrier after 5 h of incubation	S22
Tab. S4	Accumulation of (3*S*,3'*S*)-AXT in adipocytes over time.	S22

Search: search1 (Wed May 24 17:18:10 2023): Hits 1-4

BAHYEP01

Reference: G.Bartalucci, J.Coppin, S.Fisher, G.Hall, J.R.Helliwell, M.Helliwell, S.Liaaen-Jensen (2007) *Acta Crystallogr.,Sect.B:Struct.Sci.* ,**63**,328

Formula: $C_{40}H_{52}O_4$

Compound Name: 3,3'-Dihydroxy-β,β-carotene-4,4'-dione

Synonym: Astaxanthin

Space Group: P-1 **Cell:** **a** 8.537(1) **b** 8.663(1) **c** 13.298(1)
Space Group No.: 2 **(Å,°)** α 95.14(0) β 107.41(0) γ 98.77(0)

R-Factor (%): 5.18 **Temperature(K):** 100 **Density(g/cm³):** 1.080

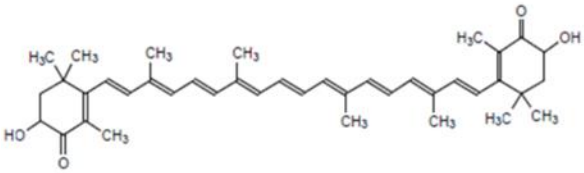

HOYXOJ

Reference: G.Bartalucci, S.Fisher, J.R.Helliwell, M.Helliwell, S.Liaaen-Jensen, J.E.Warren, J.Wilkinson (2009) *Acta Crystallogr.,Sect.B:Struct.Sci.* ,**65**,238

Formula: $C_{44}H_{56}O_6.0.44(C_4H_8O_2)$

Compound Name: 6-s-cis-Astaxanthin diacetate ethyl acetate solvate

Space Group: C2/c **Cell:** **a** 12.967(1) **b** 10.788(1) **c** 30.264(4)
Space Group No.: 15 **(Å,°)** α 90.00 β 101.80(0) γ 90.00

R-Factor (%): 8.54 **Temperature(K):** 100 **Density(g/cm³):** 1.153

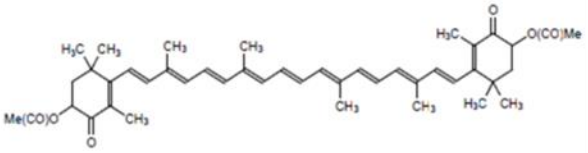

MeCO—OEt

HOYXUP

Reference: G.Bartalucci, S.Fisher, J.R.Helliwell, M.Helliwell, S.Liaaen-Jensen, J.E.Warren, J.Wilkinson (2009) *Acta Crystallogr.,Sect.B:Struct.Sci.* ,**65**,238

Formula: $C_{44}H_{56}O_6$

Compound Name: 6-s-trans-Astaxanthin diacetate

Space Group: P21/c **Cell:** **a** 10.660(1) **b** 10.168(1) **c** 18.294(1)
Space Group No.: 14 **(Å,°)** α 90.00 β 100.70(0) γ 90.00

R-Factor (%): 6.53 **Temperature(K):** 100 **Density(g/cm³):** 1.161

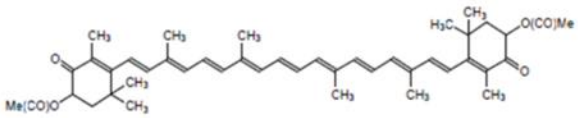

HOYYAW

Reference: G.Bartalucci, S.Fisher, J.R.Helliwell, M.Helliwell, S.Liaaen-Jensen, J.E.Warren, J.Wilkinson (2009) *Acta Crystallogr.,Sect.B:Struct.Sci.* ,**65**,238

Formula: $C_{40}H_{50}O_4$

Compound Name: (3S,3'S)-3,3'-Dihydroxy-7,8-didehydro-β,β-carotene-4,4'-dione

Synonym: (3S,3'S)-7,8-Didehydroastaxanthin

Space Group: P1 **Cell:** **a** 7.782(0) **b** 9.958(0) **c** 11.416(0)
Space Group No.: 1 **(Å,°)** α 88.13(0) β 78.33(0) γ 84.34(0)

R-Factor (%): 4.59 **Temperature(K):** 100 **Density(g/cm³):** 1.146

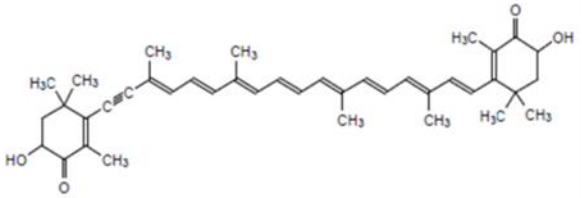

Fig. S1. The Cambridge Structural Database search results (1-4) for astaxanthin and its derivatives' crystal structures.

Search: search1 (Wed May 24 17:18:10 2023): Hits 5-7

HOYYEA

Reference: G.Bartalucci, S.Fisher, J.R.Helliwell, M.Helliwell, S.Liaaen-Jensen, J.E.Warren, J.Wilkinson (2009) *Acta Crystallogr.,Sect.B:Struct.Sci.* ,**65**,238

Formula: $C_{40}H_{48}O_4$

Compound Name: (3S,3'S)-3,3'-Dihydroxy-7,7',8,8'-tetradehydro-β,β-carotene-4,4'-dione

Synonym: (3S,3'S)-7,7',8,8'-Tetrahydroastaxanthin

Space Group:	P1	***Cell:***	***a*** 7.477(1)	***b*** 10.473(1)	***c*** 11.633(2)
Space Group No.:	1	***(Å,°)***	α 75.61(0)	β 85.90(0)	γ 76.39(0)
R-Factor (%):	4.20	***Temperature(K):***	100	***Density(g/cm³):***	1.148

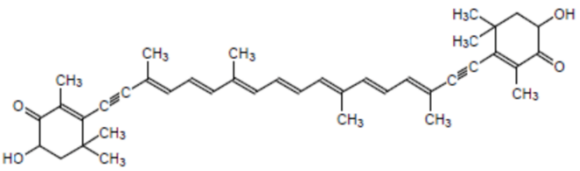

XEZJAO

Reference: G.Bartalucci, J.Coppin, S.Fisher, G.Hall, J.R.Helliwell, M.Helliwell, S.Liaaen-Jensen (2007) *Acta Crystallogr.,Sect.B:Struct.Sci.* ,**63**,328

Formula: $C_{40}H_{52}O_4,2(C_1H_1Cl_3)$

Compound Name: 3,3'-Dihydroxy-β,β-carotene-4,4'-dione chloroform solvate

Synonym: Astaxanthin chloroform solvate

Space Group:	P-1	***Cell:***	***a*** 5.959(0)	***b*** 11.858(1)	***c*** 15.647(2)
Space Group No.:	2	***(Å,°)***	α 79.04(0)	β 80.50(0)	γ 82.51(0)
R-Factor (%):	4.77	***Temperature(K):***	100	***Density(g/cm³):***	1.303

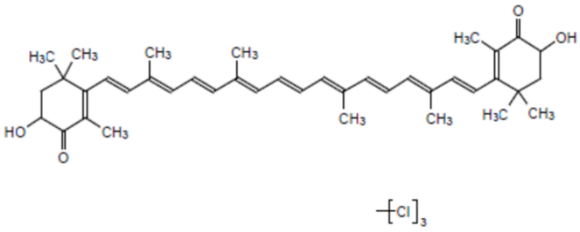

XEZJES

Reference: G.Bartalucci, J.Coppin, S.Fisher, G.Hall, J.R.Helliwell, M.Helliwell, S.Liaaen-Jensen (2007) *Acta Crystallogr.,Sect.B:Struct.Sci.* ,**63**,328

Formula: $C_{40}H_{52}O_4,2(C_5H_5N_1)$

Compound Name: 3,3'-Dihydroxy-β,β-carotene-4,4'-dione pyridine solvate

Synonym: Astaxanthin pyridine solvate

Space Group:	P21/n	***Cell:***	***a*** 18.568(4)	***b*** 6.193(1)	***c*** 19.803(4)
Space Group No.:	14	***(Å,°)***	α 90.00	β 107.75(0)	γ 90.00
R-Factor (%):	4.85	***Temperature(K):***	100	***Density(g/cm³):***	1.156

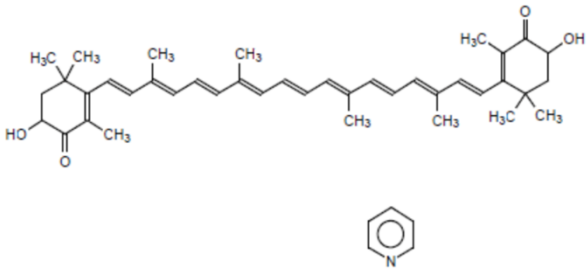

Fig. S1 (continued). The Cambridge Structural Database search results (5-7) for astaxanthin and its derivatives' crystal structures.

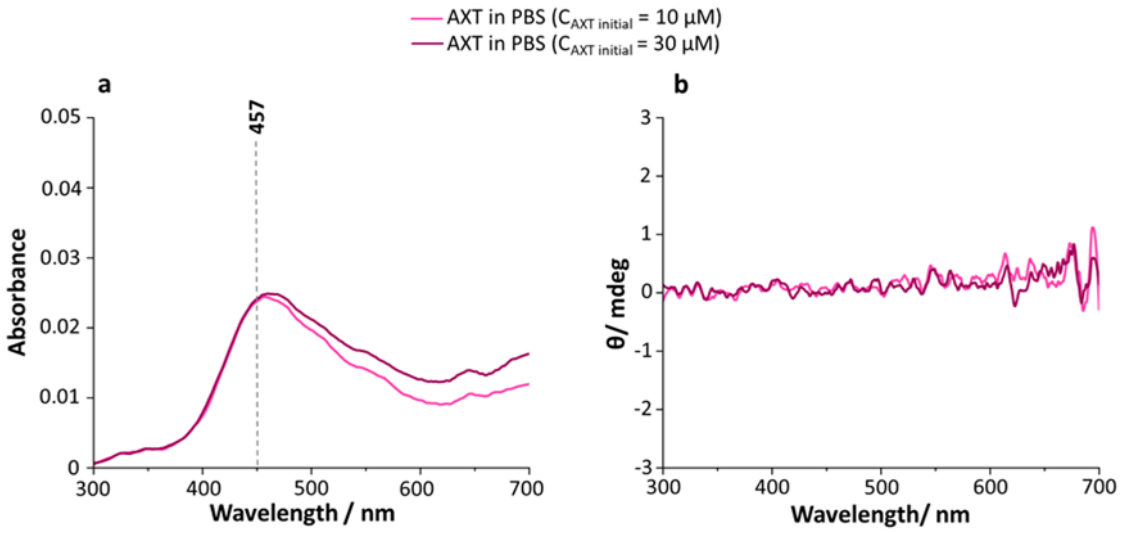

Fig. S2. Electronic absorption and ECD spectra of (3S,3'S)-AXT in PBS (after centrifugation) in the 300-700 nm range. Electronic absorption (a) and ECD (b) spectra of (3S,3'S)-AXT in PBS (without the addition of BSA) were measured for two initial (i.e., before the centrifugation) molar concentrations AXT equal to 10 and 30 μM (C_{AXT} = 10 and 30 μM).

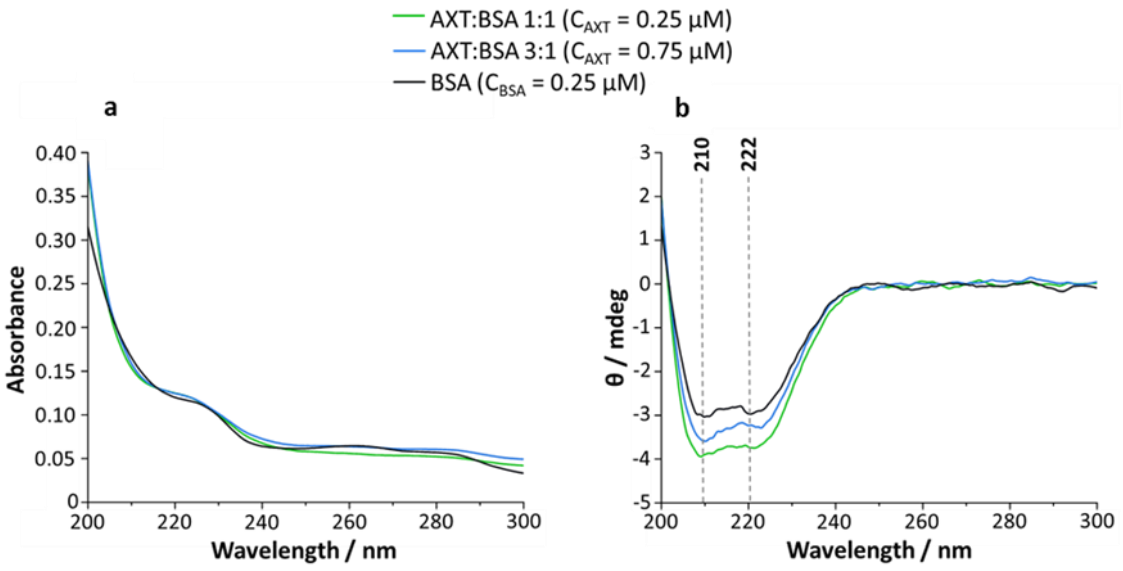

Fig. S3. Electronic absorption and ECD spectra of (3*S*,3'*S*)-AXT:BSA complexes and BSA in the 200-300 nm range. Electronic absorption (a) and ECD (b) spectra of (3*S*,3'*S*)-AXT:BSA complexes were measured for two molar ratios of AXT to BSA equal to 1:1 and 3:1, and for BSA alone at the same concentration. All solutions were diluted 40-fold before the measurement to keep the absorbance below 1.5 ($C_{AXT\ FINAL}$ = 0.25 μM, 0.75 μM; $C_{BSA\ FINAL}$=0.25 μM).

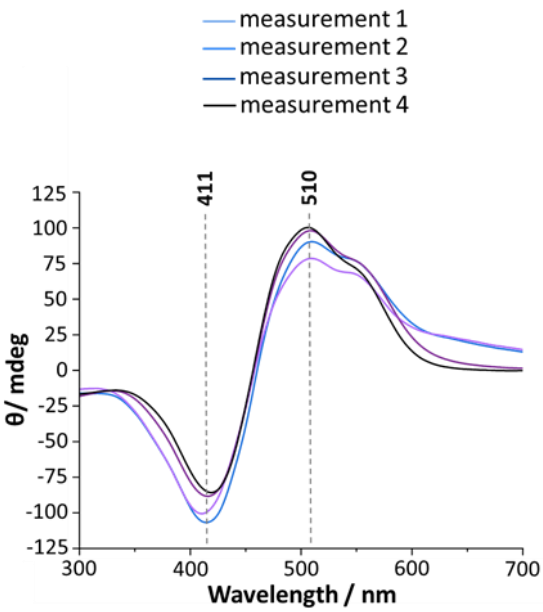

Fig. S4. ECD spectra of (3*S*,3'*S*)-AXT:BSA complexes with a molar ratio of AXT to BSA equal to 3:1 (C_{AXT} = 30 μM, C_{BSA} = 10 μM) of several independently prepared samples. Minor intensity differences between individual measurements, most likely related to the influence of external factors (e.g., temperature) which is characteristic for supramolecular systems showing high rotational and translational freedom.

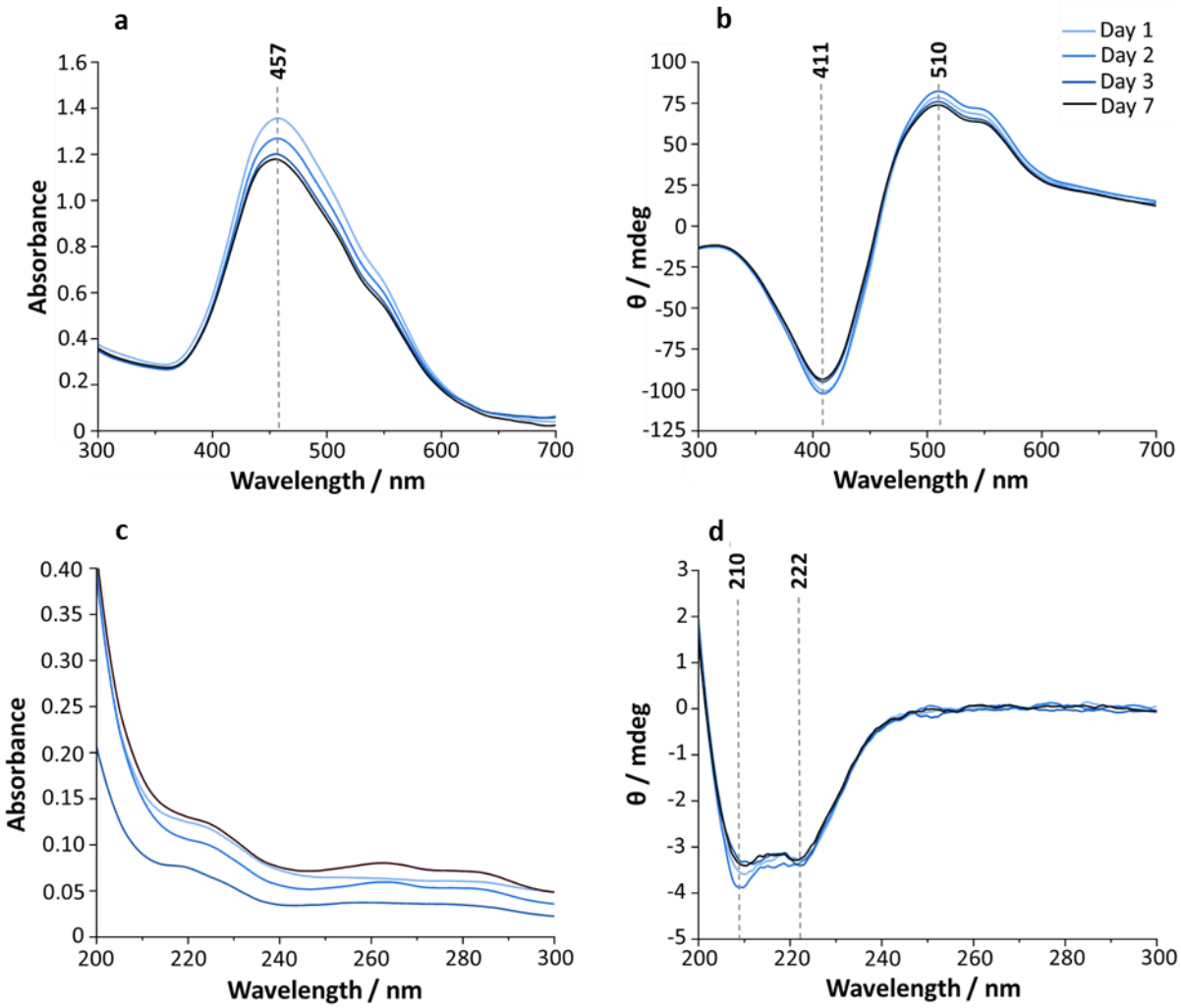

Fig. S5. Stability of the (3*S*,3'*S*)-AXT:BSA supramolecular complex monitored by electronic absorption and ECD spectra in the 700-300 nm and 300-200 nm ranges. Electronic absorption (a,c) and ECD (b,d) spectra of the (3*S*,3'*S*)-AXT:BSA complex with a molar ratio of AXT to BSA equal to 3:1 during 7 days in the 700-300 nm and in the 300-200 nm ranges, respectively. Each day, a new portion of the sample was taken for measurements and diluted 40 times to keep the absorbance below 1.5 for the 200-300 nm range ($C_{AXT\ FINAL}$ = 0.75 μM, $C_{BSA\ FINAL}$ = 0.25 μM) or measured directly for the 300-700 nm range ($C_{AXT\ FINAL}$ = 30 μM, $C_{BSA\ FINAL}$ = 10 μM).

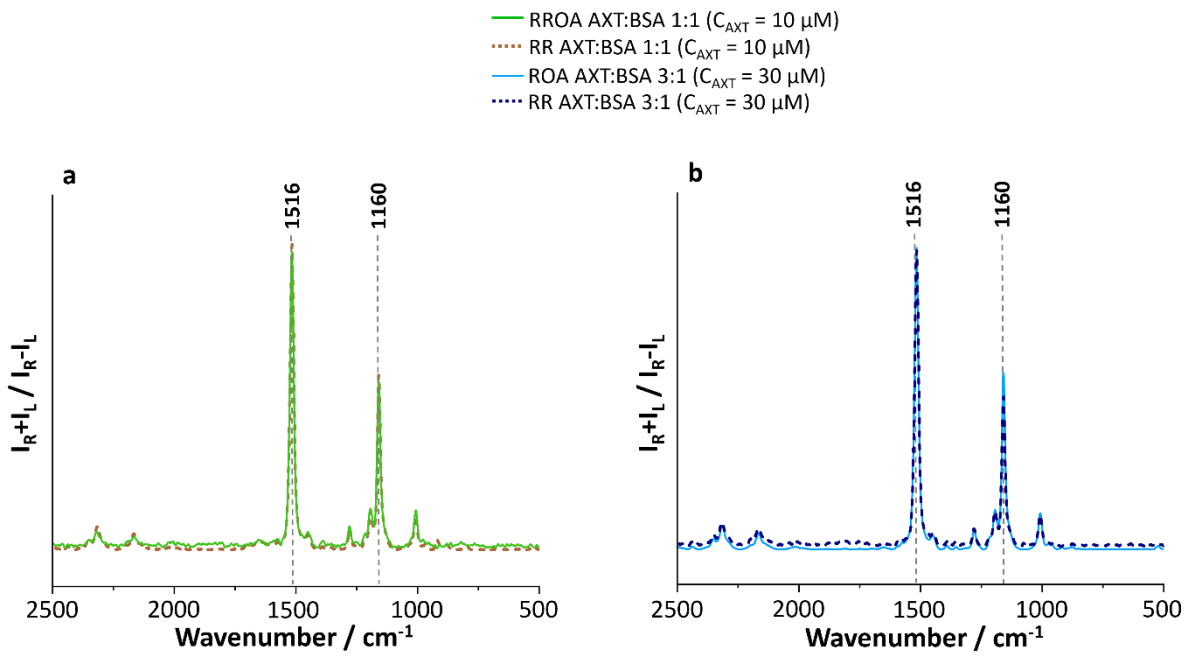

Fig. S6. Comparison of reversed RROA and RR spectra for (3*S*,3'*S*)-AXT:BSA complexes. RROA and RR spectra (normalized in the range 1570-1470 cm^{-1} to have the same peak intensity of the AXT marker band near 1516 cm^{-1}) compared for the complex with a AXT:BSA molar ratio of 1:1 (a) and 3:1 (b) (C_{AXT} = 10 and 30 μM, C_{BSA} = 10 μM).

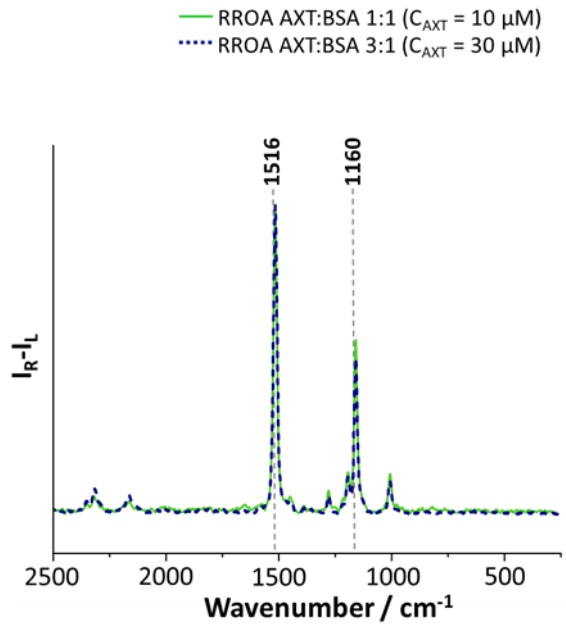

Fig. S7. Comparison of reversed RROA spectra for (3*S*,3'*S*)-AXT:BSA complexes with 1:1 and 3:1 CAR to BSA molar ratio. Spectra for both complexes (C_{AXT} = 10 and 30 μM, C_{BSA} = 10 μM) were normalized in the range 1570-1470 cm^{-1} to have the same peak intensity of the AXT marker band near 1516 cm^{-1}.

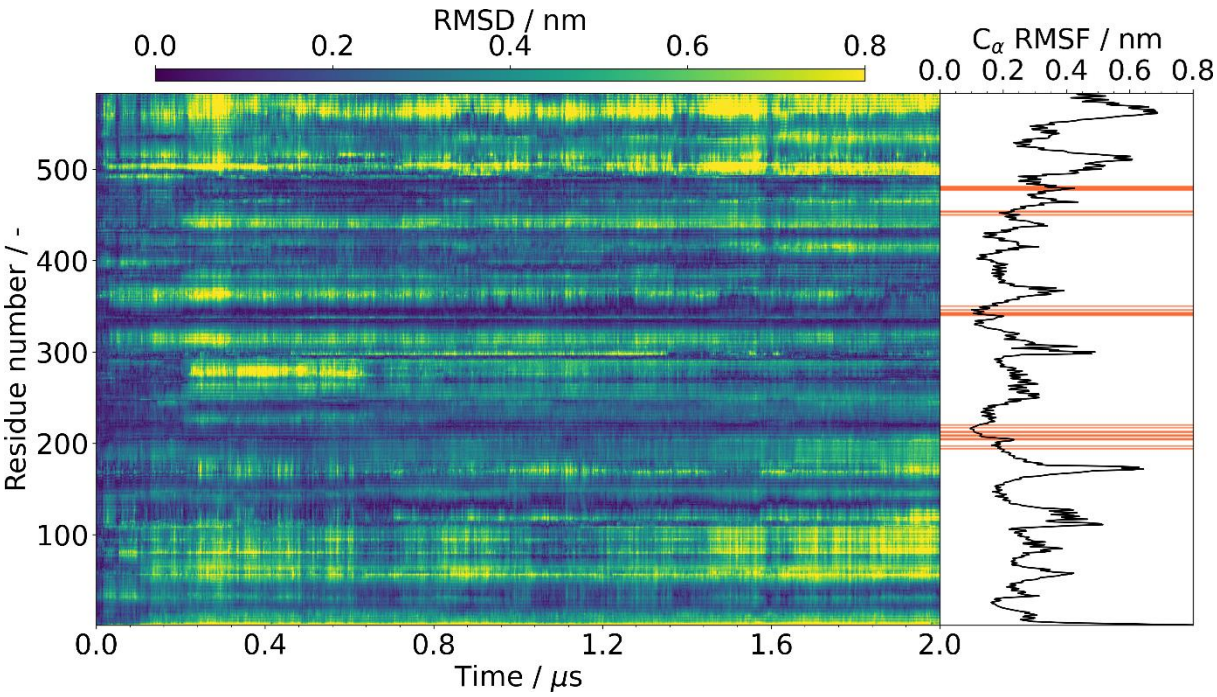

Fig. S8. Root mean square displacement (RMSD) of Cα of the BSA residues as a function of physical time and respective RMSF for the 1:1 system. On the root mean square fluctuation (RMSF) plot, the orange lines represent the residues in the binding pocket.

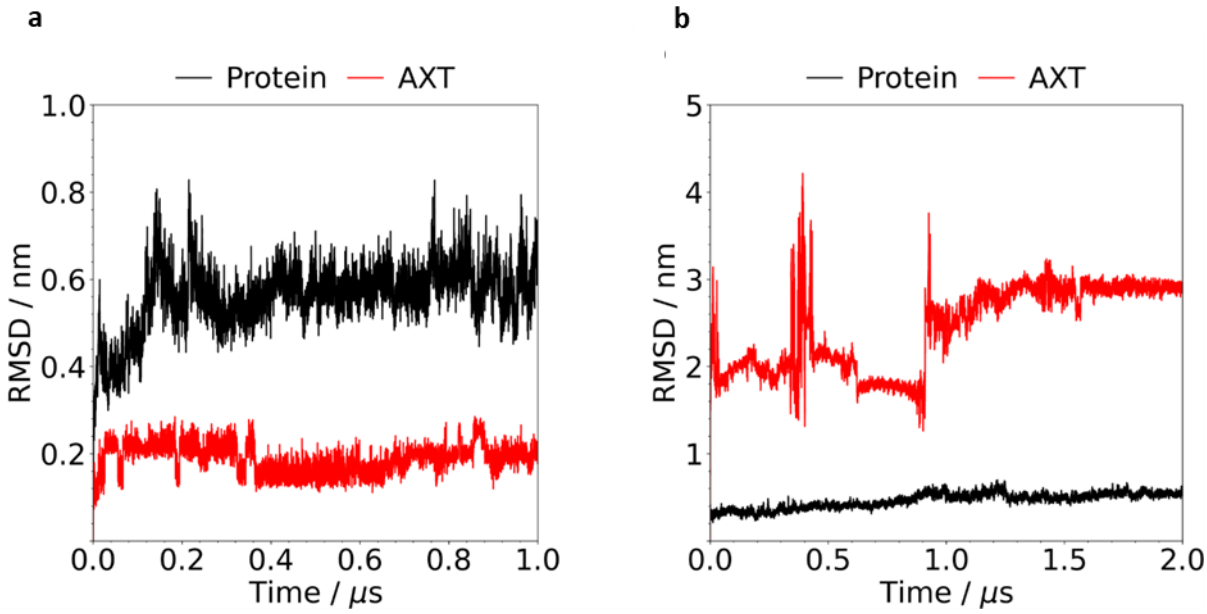

Fig. S9. RMSD of BSA backbone and (3*S*,3'*S*)-AXT molecules.(a) – (3*S*,3'*S*)-AXT:BSA = 1:1; (b) – (3*S*,3'*S*)-AXT:BSA = 3:1. Notice the difference in the ordinate scales.

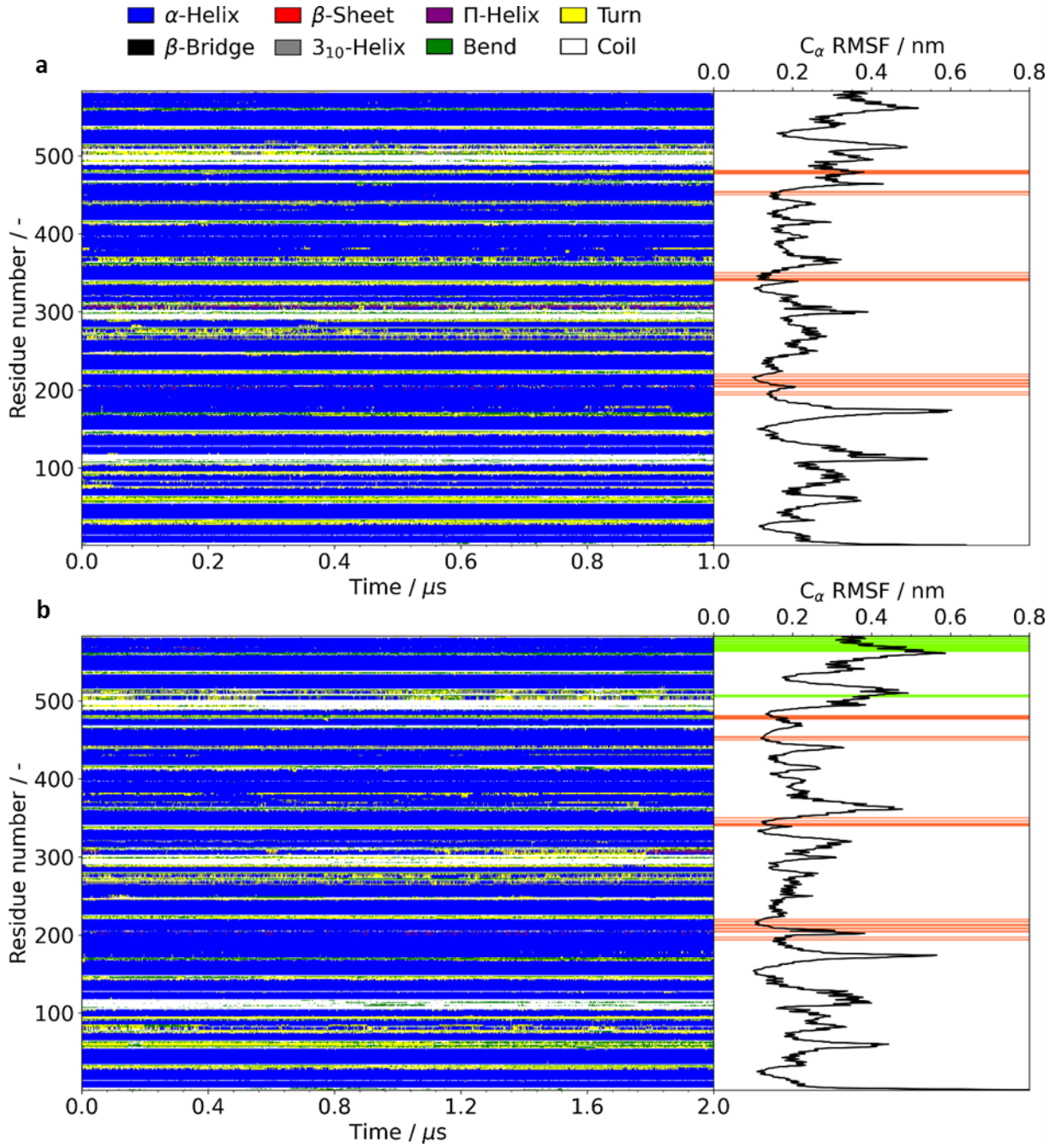

Fig. S10. Secondary structure of BSA residues as a function of physical time and respective RMSF values for the 1:1 (a) and 3:1 (b) systems. On the RMSF plots, the orange and green lines represent the residues in the binding pocket and in contact with the (3*S*,3'*S*)-AXT aggregate, respectively.

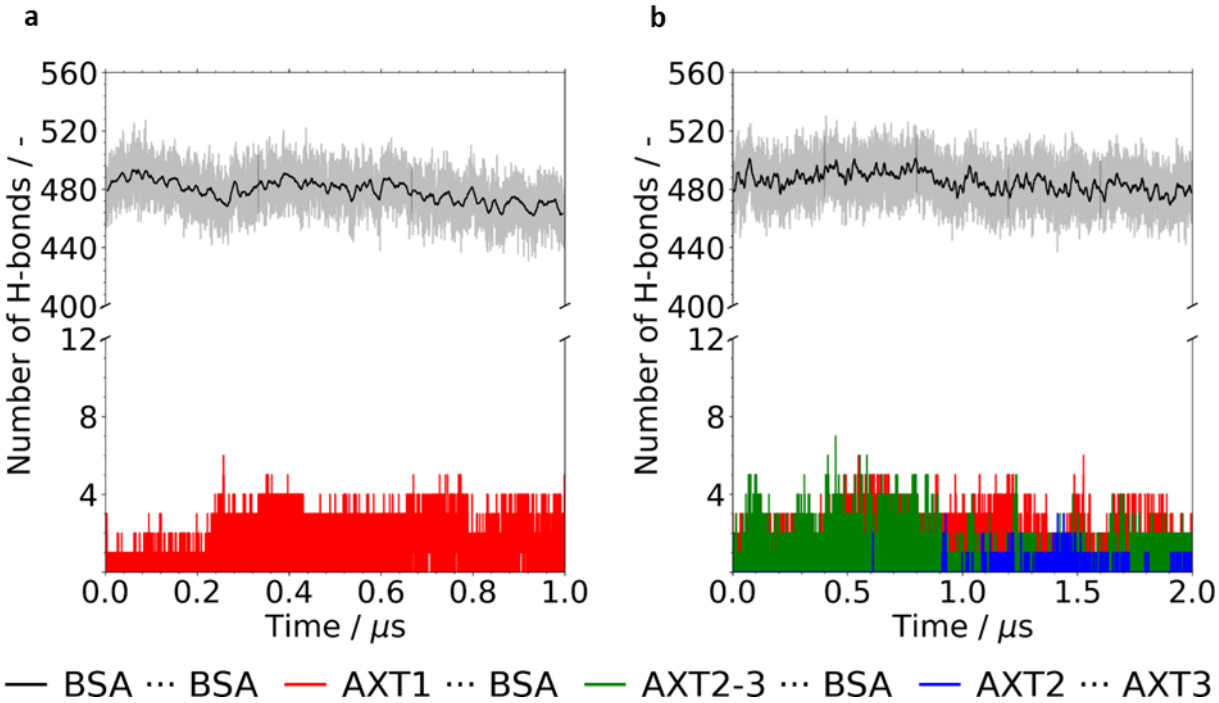

Fig. S11. Evolution of the hydrogen bonds during the simulation time. (a) – (3*S*,3'*S*)-AXT:BSA = 1:1; (b) – (3*S*,3'*S*)-AXT:BSA = 3:1. AXT1 refers to the (3*S*,3'*S*)-AXT molecule inside the binding pocket; AXT2 and AXT3 refer to the (3*S*,3'*S*)-AXT molecules in solution.

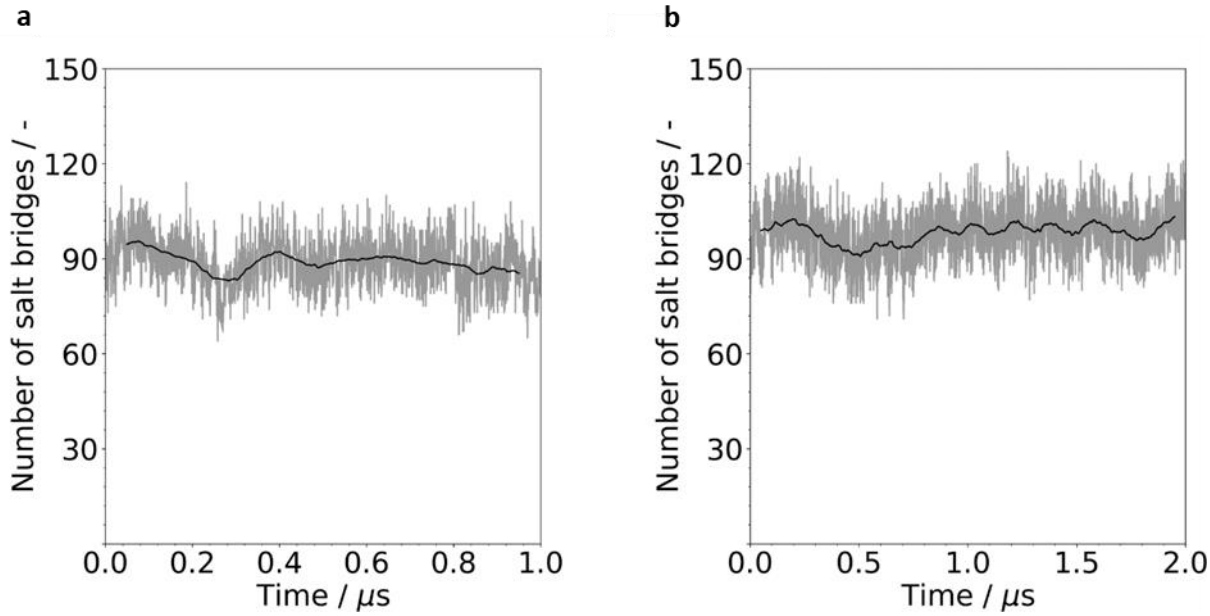

Fig. S12. Number of salt bridges in BSA as a function of physical time. (a) – (3*S*,3'*S*)-AXT:BSA = 1:1; (b) – (3*S*,3'*S*)-AXT:BSA = 3:1.

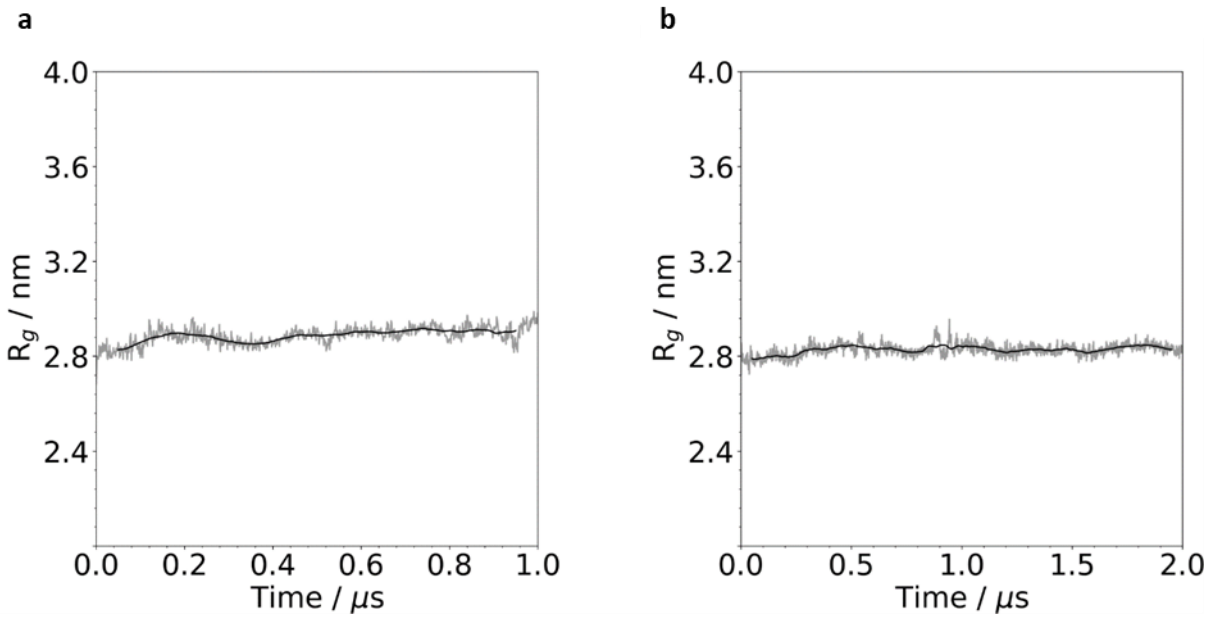

Fig. S13. Radius of gyration of BSA as a function of physical time. (a) – (3*S*,3'*S*)-AXT:BSA = 1:1; (b) – (3*S*,3'*S*)-AXT:BSA = 3:1.

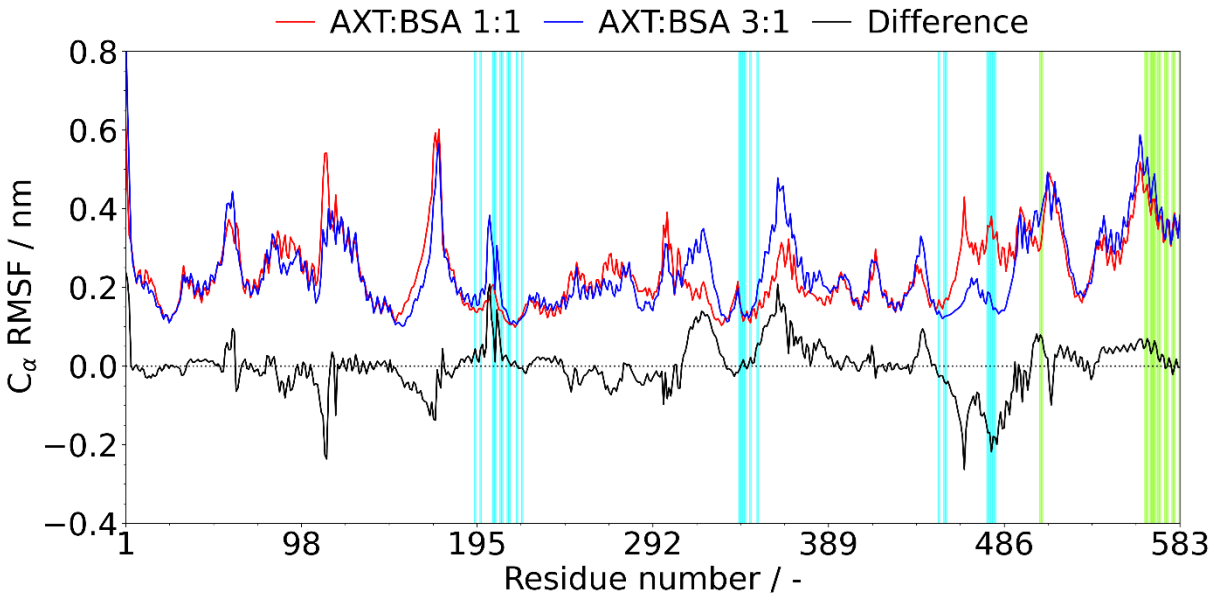

Fig. S14. Root mean square fluctuations of Cα of the BSA residues. The cyan and green lines represent the residues in the binding pocket and in contact with the (3*S*,3'*S*)-AXT aggregate, respectively.

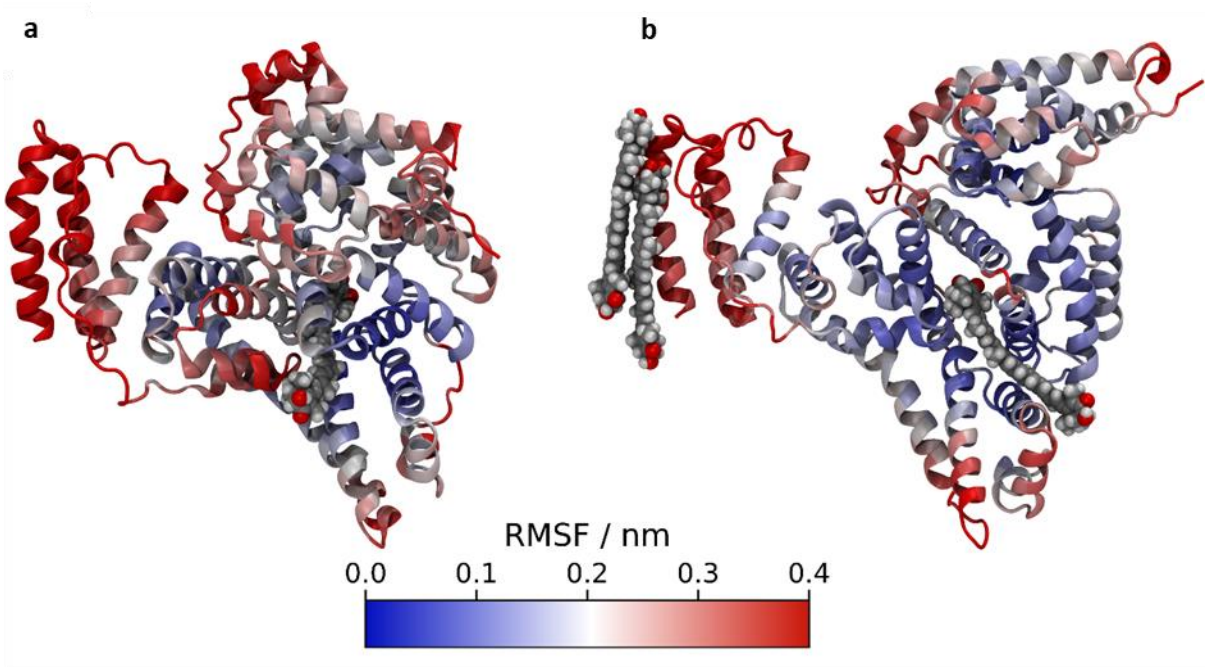

Fig. S15. Mapping of RMSF values on the BSA structure. (a) – (3*S*,3'*S*)-AXT:BSA = 1:1; (b) – (3*S*,3'*S*)-AXT:BSA = 3:1.

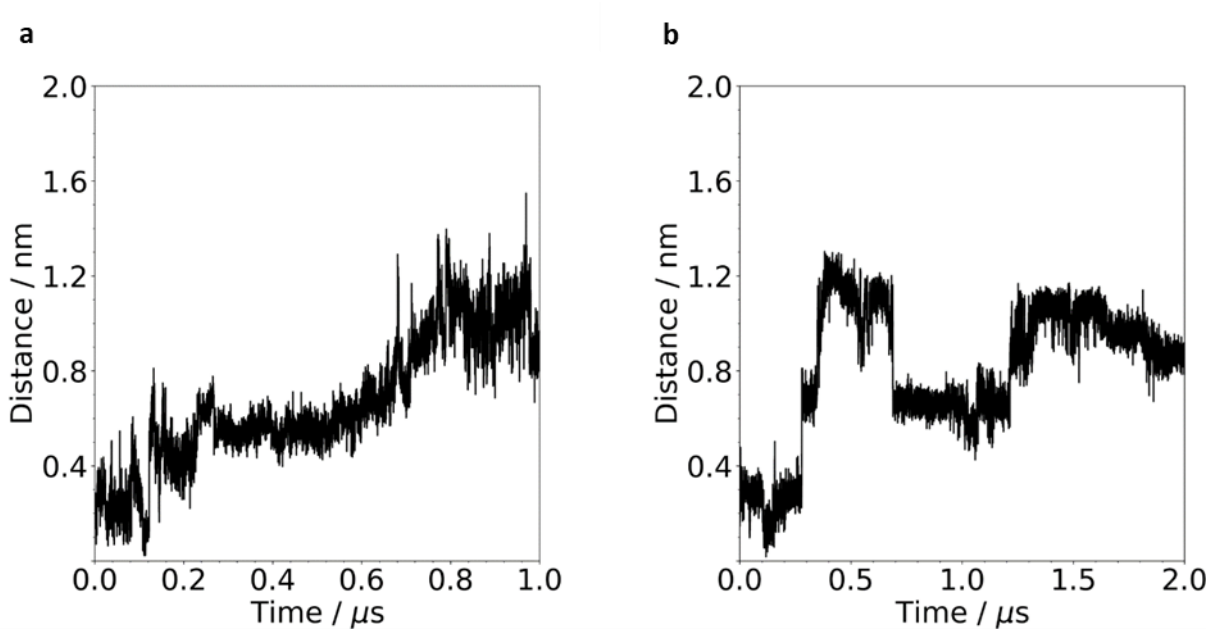

Fig. S16. Distances between the centre of mass (COM) of the bonded AXT molecule and the COM of the binding pocket residues. (a) – (3*S*,3'*S*)-AXT:BSA = 1:1; (b) – (3*S*,3'*S*)-AXT:BSA = 3:1.

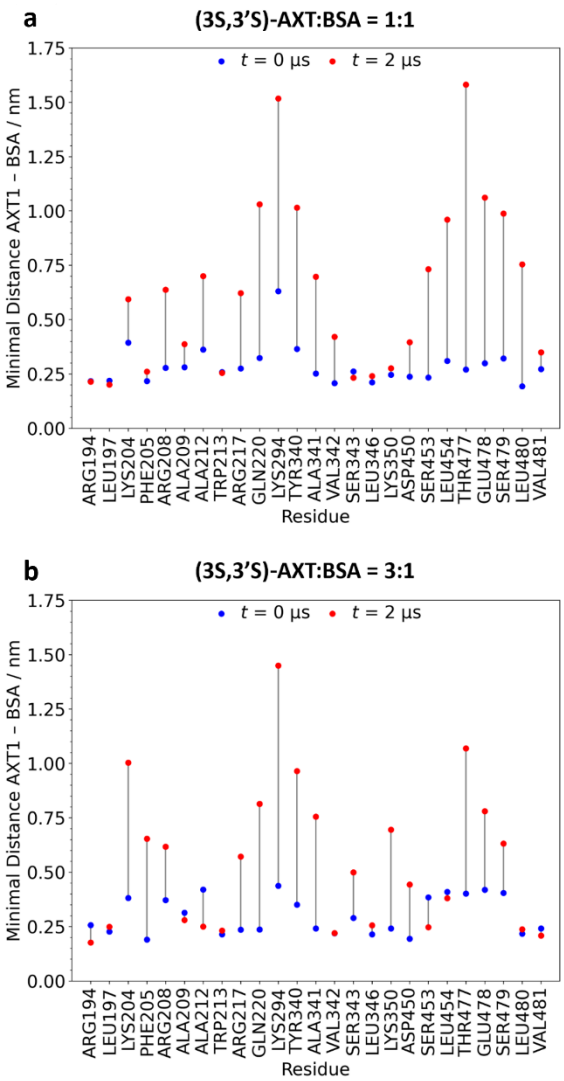

Fig. S17. Minimum distances between AXT1 (AXT in the binding pocket) and selected residues of the BSA binding pocket at the start (t = 0 μs, blue dots) and at the end (t = 2 μs, red dots) of the simulation time for: (a) (3S,3'S) AXT:BSA = 1:1 ratio; and (b) (3S,3'S)-AXT:BSA = 3:1 ratio. The average values for the minimum distances between AXT1 and the BSA binding pocket residues for the (3S,3'S)-AXT:BSA = 1:1 system are 0.30 nm (t = 0 μs) and 0.55 nm (t = 2 μs), while for the (3S,3'S)-AXT:BSA = 3:1 system they are 0.29 nm (t = 0 μs) and 0.64 nm (t = 2 μs).

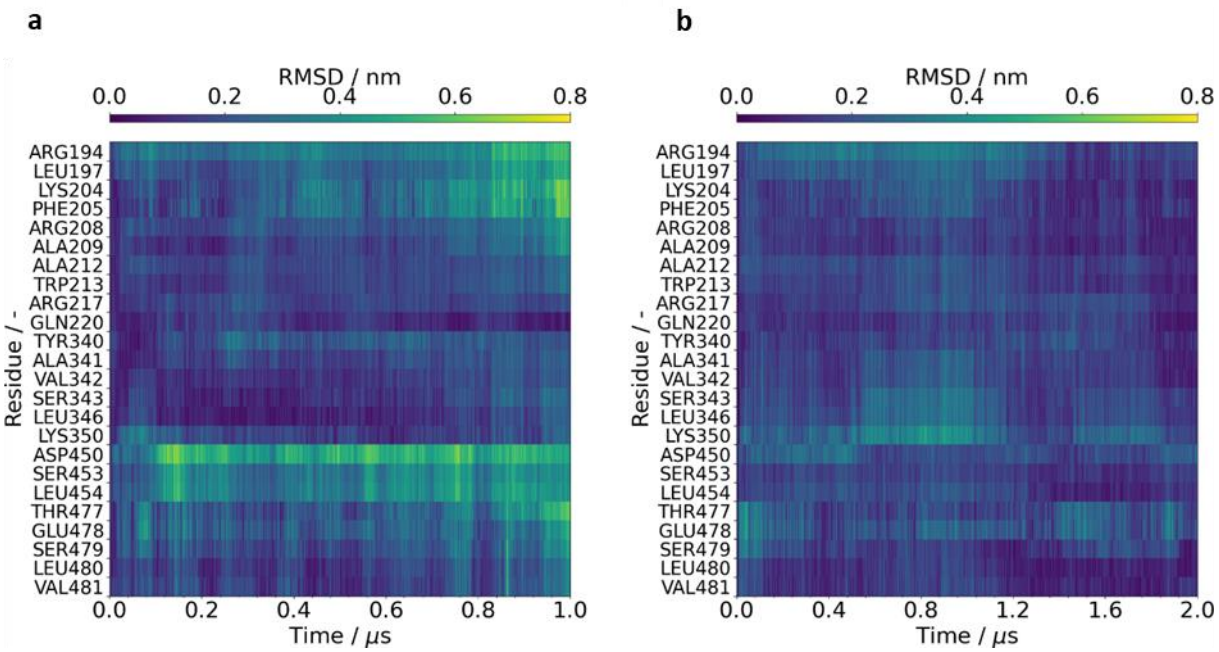

Fig. S18. RMSD of Cα of the BSA regarding the binding pocket residues. (a) – (3*S*,3'*S*)-AXT:BSA = 1:1; (b) – (3*S*,3'*S*)-AXT:BSA = 3:1.

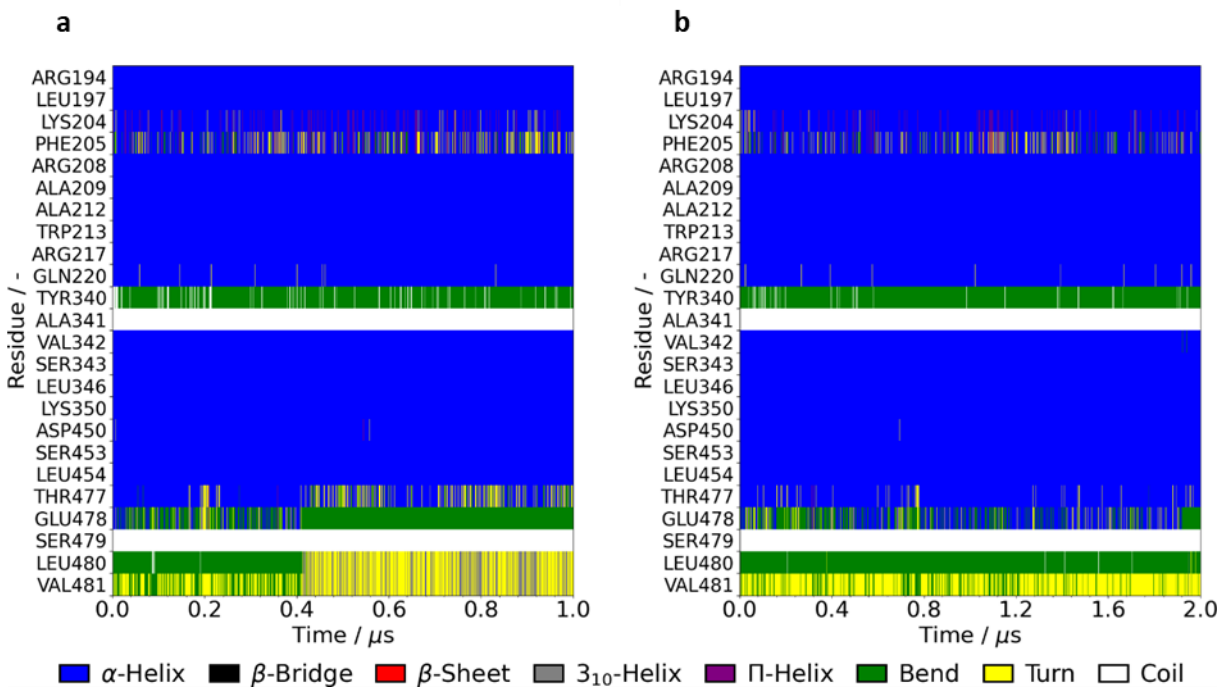

Fig. S19. Secondary structure of the BSA regarding the binding pocket residues. (a) – (3*S*,3'*S*)-AXT:BSA = 1:1; (b) – (3*S*,3'*S*)-AXT:BSA = 3:1.

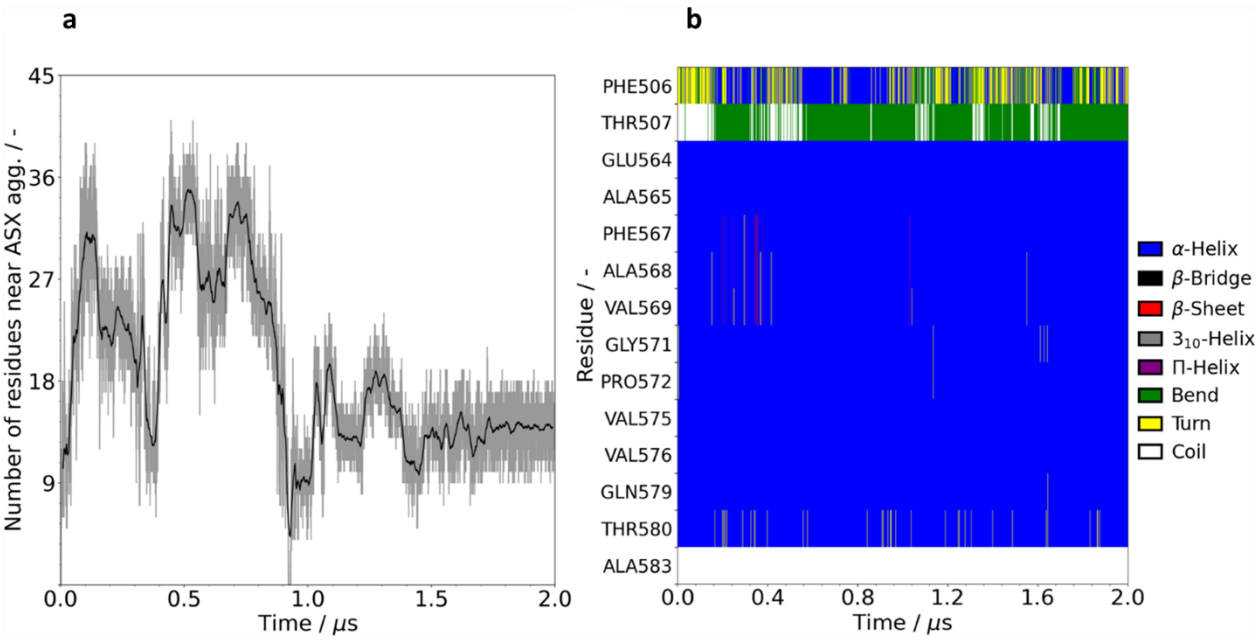

Fig. S20. (a) Number of BSA residues in contact with the two (3*S*,3'*S*)-AXT molecules in solution; (b) Secondary structure of BSA regarding the residues in contact with (3*S*,3'*S*)-AXT aggregate. The latter residues have been identified in the trajectory with a cut-off of 0.45 nm for the interval 1.6-2.0 μs.

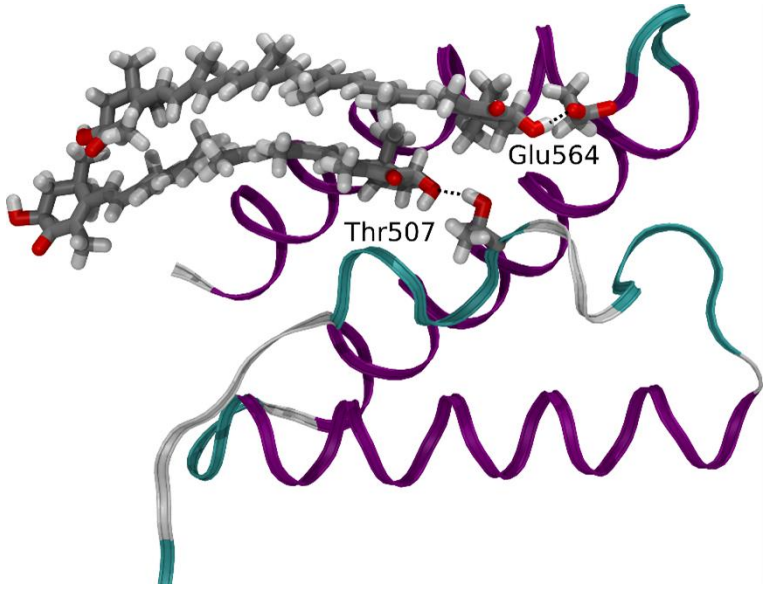

Fig. S21. Hydrogen bonds between the (3*S*,3'*S*)-AXT aggregate and BSA residues.

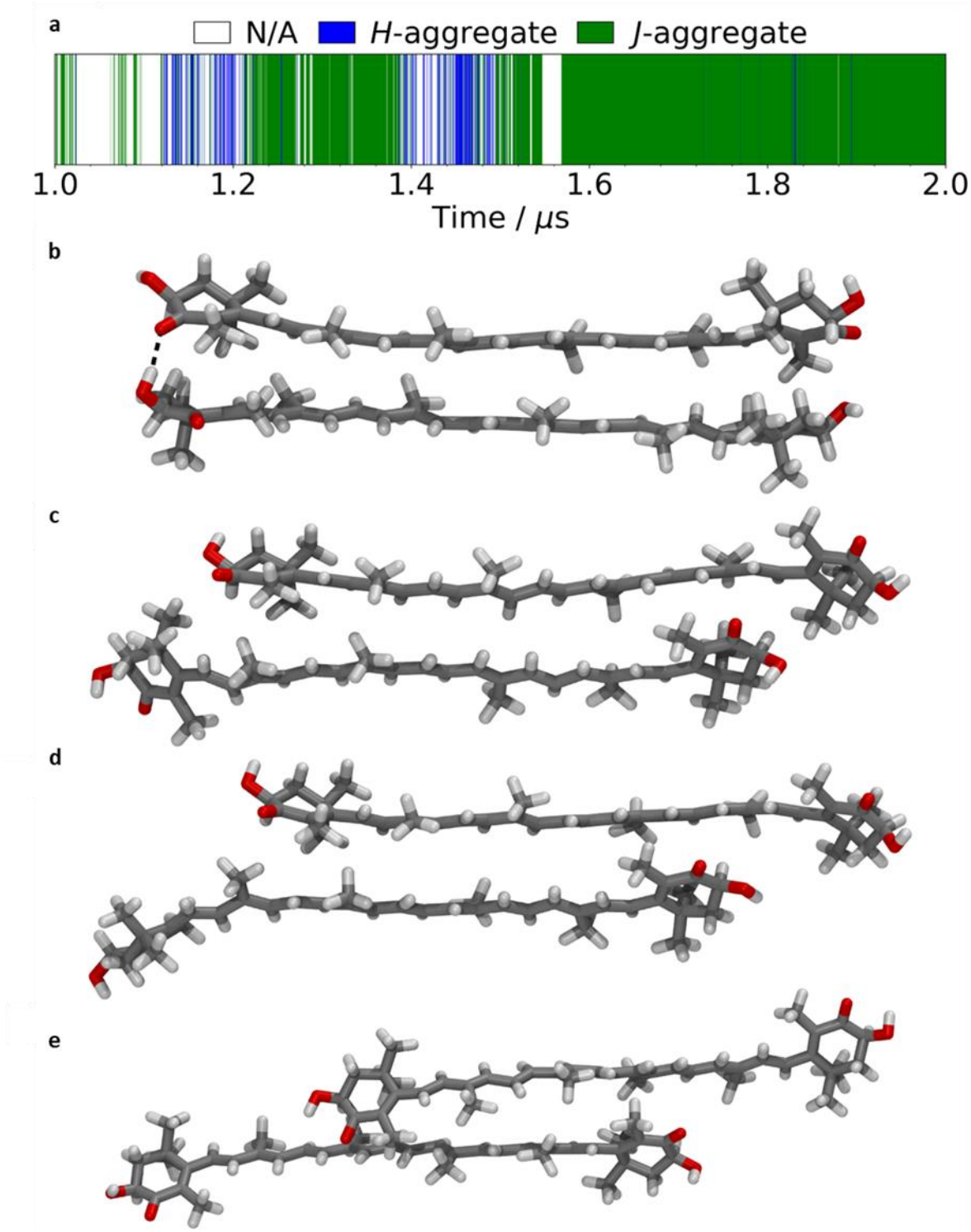

Fig. S22. Classification and illustration of the (3*S*,3'*S*)-AXT aggregates observed in the last μs of the trajectory. (a) – Classification of the (3*S*,3'*S*)-AXT aggregates as a function of the time. "The classification was performed by extracting from the trajectory a representative structure of the *H*-aggregate (b), and three representative *J*-aggregate conformations (c-e) with different distances between the COM for each (3*S*,3'*S*)-AXT molecule in the pair. Then RMSD of the aggregate relative to each of these structures was computed for the same time interval. Finally, the aggregate conformations in each frame were classified as *H*- or *J*- type if the respective RMSD fell below a given cut-off."

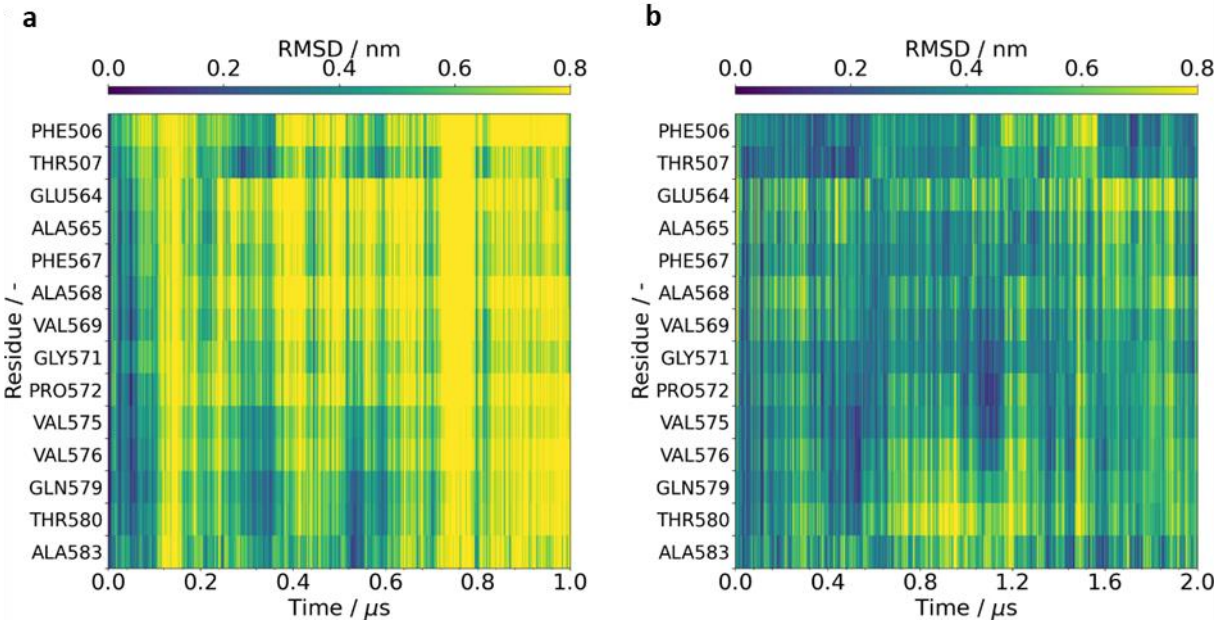

Fig. S23. RMSD of Cα of the BSA residues in contact with the (3*S*,3'*S*)-AXT aggregate observed for the 3:1 system. (a) – (3*S*,3'*S*)-AXT:BSA = 1:1 (for comparison); (b) – (3*S*,3'*S*)-AXT:BSA = 3:1.

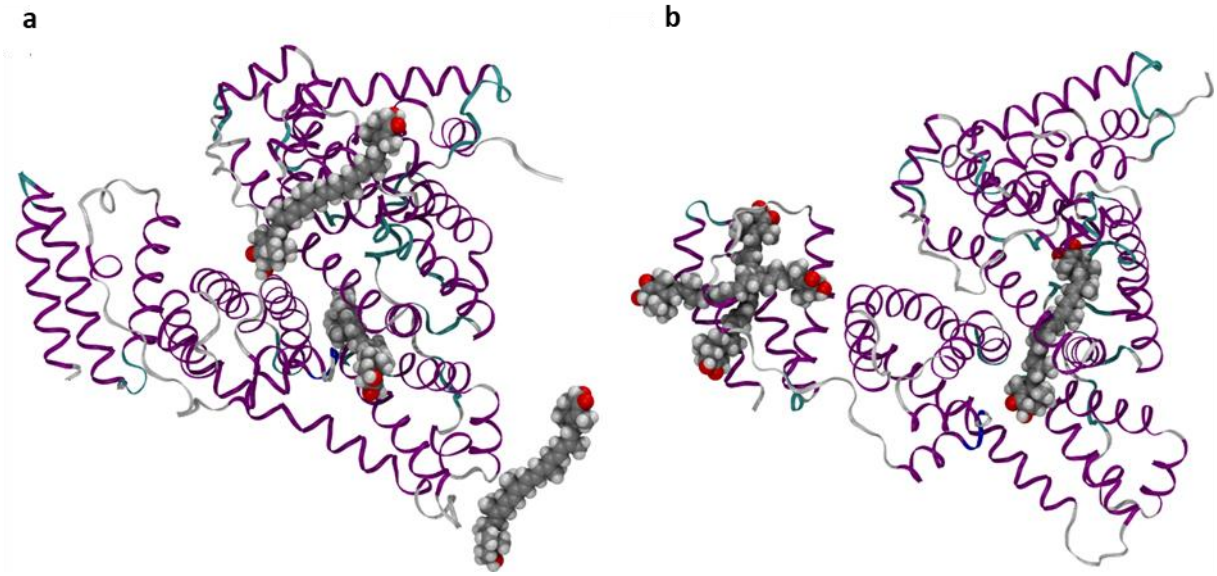

Fig. S24. Initial and final frames from the trajectory of an MD simulation for the 3:1 (3*S*,3'*S*)-AXT:BSA system without restraining the dihedrals in the polyene chain of (3*S*,3'*S*)-AXT. (a) t = 0 μs; (b) t = 1 μs. Solvent molecules and counterions are omitted for clarity.

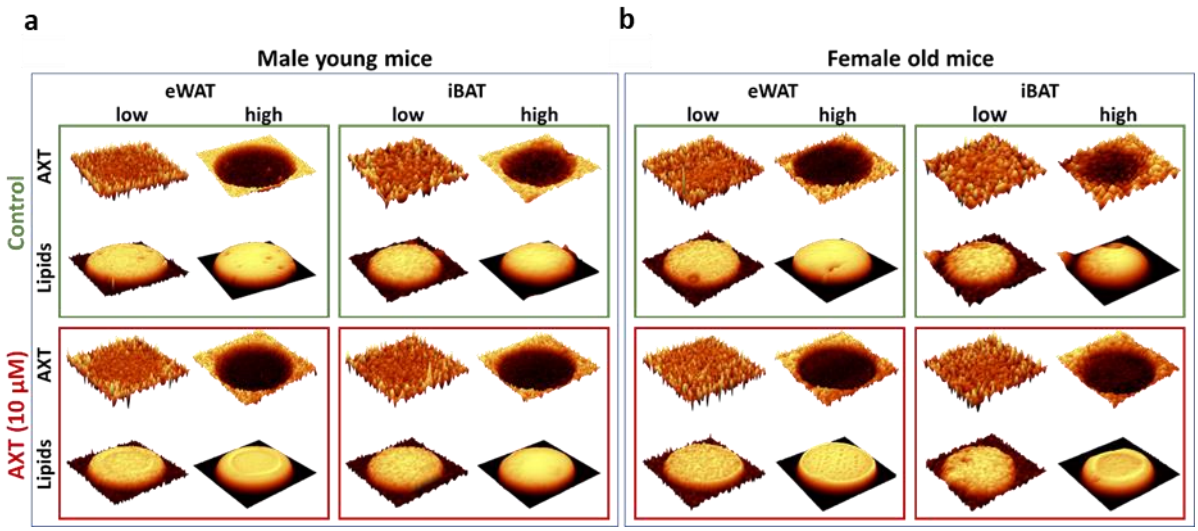

Fig. S25. Images of lipid and (3S,3'S)-astaxanthin distribution in primary adipocytes of white adipose tissue (eWAT) and brown adipose tissue (iBAT), after stimulation with (3*S*,3'*S*)-AXT dispersed in DMSO:water, for mice of different age, sex and using different laser power. Primary adipocytes of epididymal white (eWAT) and interscapular brown adipose tissue (iBAT) isolated from male young (8 weeks, a) and female old (43 weeks, b) mice were measured using low and high (ca. 3 mW and 30 mW, respectively) laser power. Images for the control group and cells stimulated with (3*S*,3'*S*)-AXT in DMSO:water dispersion were obtained by the integration in the marker bands for AXT (1535−1505 cm^{-1}) and lipids (2900−2830 cm^{-1}).

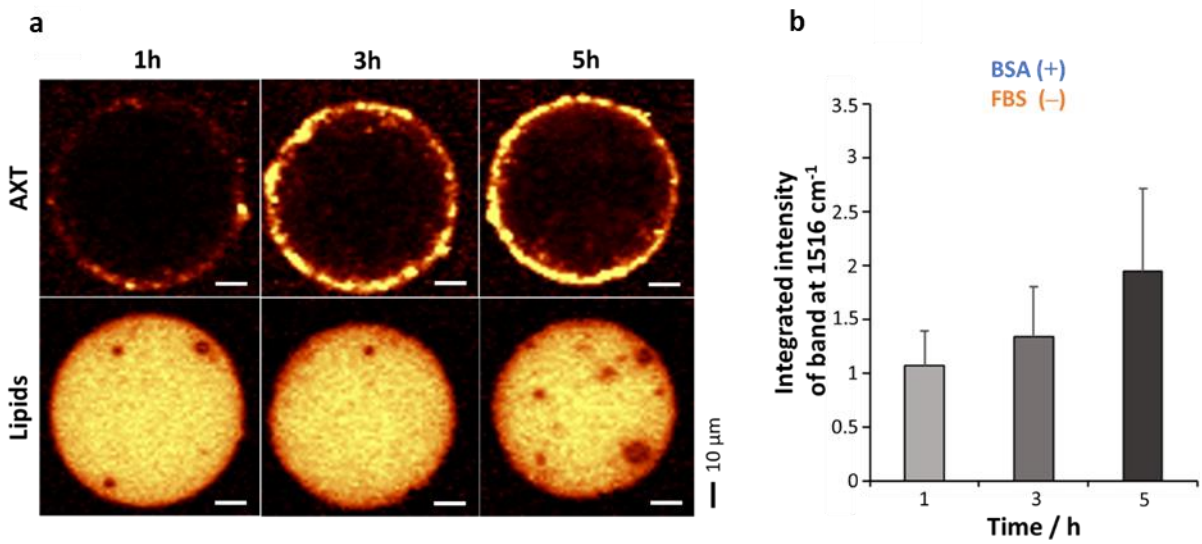

Fig. S26. Time-dependent increase of AXT level in primary adipocytes. Representative Raman images of the (3*S*,3'*S*)-AXT (1535−1505 cm^{-1}) and lipids (2900−2830 cm^{-1}) from selected time points (a) and the degree of AXT accumulation (I_{1516}) inside adipocytes excluding the cell edges (n = 3 per time point) (b) were shown. Error bars represent standard errors. Cells were incubated with (3*S*,3'*S*)-AXT:BSA complex. The cell culture medium did not contain fetal bovine serum (FBS). Scale bars are equal to 10 µm.

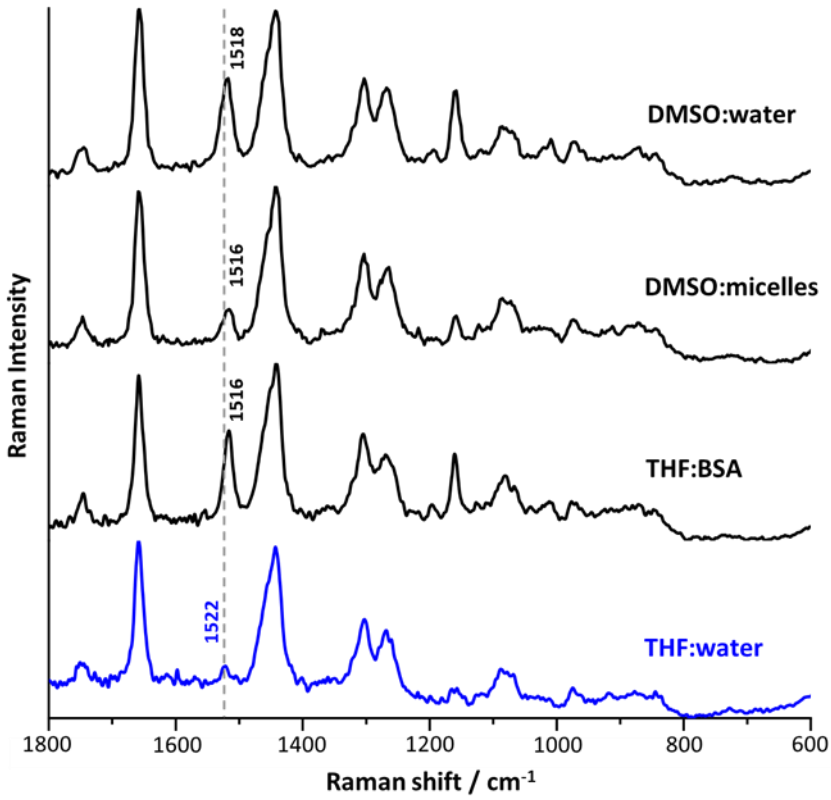

Fig. S27. Changes in the position of marker band near 1516 cm^{-1} due to different forms of (3*S*,3'*S*)-AXT delivery. Average Raman spectra for each set were normalized in the 1800–600 cm^{-1} spectral range. Primary adipocytes were incubated with (3*S*,3'*S*)-AXT for 3 h. The cell culture media with DMSO contained FBS whereas the ones with THF did not.

Tab. S1. Ratios of the experimental integrated intensity of the bands at 1516 cm^{-1} and 1160 cm^{-1} (I_{1516}/I_{1160}) for RR and RROA spectra for (3*S*,3'*S*)-AXT to BSA molar ratios of 1:1 and 3:1.

	AXT:BSA = 1:1	**AXT:BSA = 3:1**
RR	1.53	1.55
RROA	1.63	1.90

Tab. S2. Experimental ratios of CID values for bands at 1516 and 1160 cm^{-1}. CID values were obtained by dividing the experimental integral intensity of the respective bands in the RROA and RR spectra ($I_{1516\ RROA}/I_{1516\ RR}$, $I_{1160\ RROA}/I_{1160\ RR}$) for both (3*S*,3'*S*)-AXT:BSA complexes with molar ratios of 1:1 and 3:1.

	AXT:BSA = 1:1	**AXT:BSA = 3:1**
$I_{1516\ RROA}$ / $I_{1516\ RR}$	$-2.64 \cdot 10^{-3}$	$-2.94 \cdot 10^{-3}$
$I_{1160\ RROA}$ / $I_{1160\ RR}$	$-2.49 \cdot 10^{-3}$	$-2.40 \cdot 10^{-3}$

Tab. S3. Comparison of (3*S*,3'*S*)-AXT content in adipocytes depending on the presence of BSA as a carrier after 5 h of incubation. The amount of AXT was estimated using the integral intensity of the marker band for AXT near 1520 cm^{-1} (I_{1520}) after incubation of adipocytes with [BSA(+),FBS(−)] and [BSA(−),FBS(−)] systems.

I_{1520}	**BSA(+) FBS(−)**	**BSA(−) FBS(−)**
	1.48	0.56

Tab. S4. Accumulation of (3*S*,3'*S*)-AXT in adipocytes over time. The amount of AXT over time was estimated using the integral intensity of the marker band for AXT near 1520 cm^{-1} (I_{1520}) at a given time point, after incubation of adipocytes with AXT:BSA complex [BSA(+),FBS(−)].

I_{1520}	**Time / h**		
	1	**3**	**5**
	0.77	1.33	1.48